Three-Dimensional Augmented Reality Visualization Informs Locoregional Therapy in a Translational Model of Hepatocellular Carcinoma

Brian J. Park, MD, Nicholas R. Perkons, BS, Enri Profka, BS, Omar Johnson, MS, Christopher Morley, MD, Scott Appel, MS, Gregory J. Nadolski, MD, Stephen J. Hunt, MD, PhD, and Terence P. Gade, MD, PhD

ABSTRACT

Purpose: To evaluate the utility of visualizing preprocedural MR images in 3-dimensional (3D) space using augmented reality (AR) before transarterial embolization of hepatocellular carcinoma (HCC) in a preclinical model.

Materials and Methods: A total of 28 rats with diethylnitrosamine-induced HCCs > 5 mm treated with embolization were included in a prospective study. In 12 rats, 3D AR visualization of preprocedural MR images was performed before embolization. Procedural metrics including catheterization time and radiation exposure were compared vs a prospective cohort of 16 rats in which embolization was performed without AR. An additional cohort of 15 retrospective cases was identified and combined with the prospective control cohort (n = 31) to improve statistical power.

Results: A 37% reduction in fluoroscopy time, from 11.7 min to 7.4 minutes, was observed with AR when compared prospectively, which did not reach statistical significance ($P = .12$); however, when compared with combined prospective and retrospective controls, the reduction in fluoroscopy time from 14.1 min to 7.4 minutes (48%) was significant ($P = .01$). A 27% reduction in total catheterization time, from 42.7 minutes to 31.0 minutes, was also observed with AR when compared prospectively, which did not reach statistical significance ($P = .11$). No significant differences were seen in dose–area product or air kerma prospectively.

Conclusions: Three-dimensional AR visualization of preprocedural imaging may aid in the reduction of procedural metrics in a preclinical model of transarterial embolization. These data support the need for further studies to evaluate the potential of AR in endovascular oncologic interventions.

ABBREVIATIONS

AK = air kerma, AR = augmented reality, DAP = dose–area product, DICOM = Digital Imaging and Communications in Medicine, HCC = hepatocellular carcinoma, 3D = 3-dimensional, 2D = 2-dimensional

Augmented reality (AR) is an emerging display technology that can provide stereoscopic 3-dimensional (3D) views of cross-sectional imaging (1,2). The added depth information afforded by stereoscopic 3D AR may inherently enhance and improve functional neural processes for learning and comprehension, consistent with findings demonstrated with

From the Department of Radiology (B.J.P., N.R.P., E.P., O.J., S.A., G.J.N., S.J.H., T.P.G.), Perelman School of Medicine, University of Pennsylvania, 646 BRB II/III, 421 Curie Blvd., Philadelphia, PA 19104; and Medivis (C.M.), Brooklyn, New York. Received August 28, 2019; final revision received December 26, 2019; accepted January 29, 2020. Address correspondence to B.J.P.; E-mail: bjinwoopark@gmail.com; Twitter handle: @bparkmd

From the 2019 SIR Annual Meeting.

B.J.P. receives grants from Nvidia (Santa Clara, California). C.M. is the founder and chief operating officer of Medivis (Brooklyn, New York). None of the other authors have identified a conflict of interest.

Figures E1 and E2 and Videos 1 and 2 can be found by accessing the online version of this article on *www.jvir.org* and clicking on the Supplemental Material tab.

J Vasc Interv Radiol 2020; 31:1612–1618

https://doi.org/10.1016/j.jvir.2020.01.028

3D printing for surgical planning, which resulted in reduced operating room times and decreased exposure to ionizing radiation (3–5). Indeed, 3D visualization technologies have been shown to improve anatomic knowledge and test performance of medical students compared with 2-dimensional (2D) images (6).

Three-dimensional software and systems currently exist for volumetric vasculature reconstruction (7,8). However, many of these systems are limited by 3D data reduced to 2D monitor screens and often require separate workstations that are not integrated with live fluoroscopy. With AR headsets, holographic 3D data can be integrated with actual data in the interventional suite. Monitors displaying live digital subtraction angiography can be overlaid with, and matched to, holographic 3D preprocedural scans to provide depth information that is absent from the angiographic images (**Fig E1** and **Video 1** [available online on the article's Supplemental Material page at *www.jvir.org*]).

The feasibility of stereoscopic 3D visualization of cross-sectional imaging for endovascular procedures has been demonstrated with the use of preprocedural contrast-enhanced computed tomography (CT) and time-of-flight magnetic resonance (MR) angiography (7,9). However, the influence of 3D visualization with AR headsets on procedure duration and radiation exposure remain to be investigated. To determine if procedural metrics could be improved, the present study evaluated the utility of visualizing preprocedural MR images in 3D space using an AR optical see-through head-mounted display before transarterial embolization in rats.

MATERIALS AND METHODS

Study Design

The study was approved by the study institution's animal welfare and use committee. The induction of cirrhosis and hepatocellular carcinoma (HCC) in rats with the use of diethylnitrosamine and embolization via right common femoral artery access was described previously (10,11). Tumors developed in all rats, with the majority appearing within 2 weeks of completing the diethylnitrosamine diet. Rats were serially imaged, and embolization was performed when at least one tumor measured greater than 5 mm in maximum axial diameter. Only one tumor was treated in a single embolization session. Embolization was performed by one of two interventional radiologists with more than 5 years of experience working with rats.

A total of 28 prospective cases were enrolled, 12 in the AR group and 16 in the prospective control group, from August 2018 to June 2019. Rat population characteristics, including sex, weight, maximum axial tumor dimension, and liver location, were compared between the groups (**Table 1**). Procedural metrics including total catheterization time, total fluoroscopy time, dose–area product (DAP), and air kerma (AK) from prospective embolizations with and without AR were compared. Post hoc power analysis suggested a total sample size of 52 for 80% power to achieve statistical significance ($\alpha < 0.05$) with a large effect size (0.8). Because prospective comparisons were underpowered ($n = 28$), an additional 15 retrospective control cases from January 2017 to December 2017 were identified. The prospective and retrospective control cases were combined to improve power after they were determined to be statistically similar and were compared versus the AR group. Fluoroscopic guidance and angiography were performed on a Siemens Cios Alpha c-arm (Siemens Healthineers, Erlangen, Germany) for prospective cases and a Siemens SIREMOBIL Iso-C c-arm for retrospective cases. A flowchart of the study design is depicted in **Figure 1**.

Table 1. Summary of Rat Population Characteristics

Characteristic	AR (n = 12)	Control Prospective (n = 16)	*P* Value
Sex			–
Male	12	16	
Female	0	0	
Average weight (g)	464	428	.08
Liver location			.82
Left	8	12	
Right	4	5	
Average tumor maximum axial dimension (mm)	8.4	10.2	.28

Transarterial Embolization

Rats were first induced with 2% isoflurane at 1 L/min oxygen. Anesthesia was maintained with inhalation of 1.5%–2% isoflurane at 1 L/min oxygen through a nose cone. The animal was then placed in a supine position on top of a circulating water blanket, which maintained body temperature at 37°C. Body temperature was monitored throughout the procedure with the use of a rectal temperature probe. The right medial thigh and groin were shaved and cleaned with 4% chlorhexidine gluconate solution and then draped with a sterile cover. A 3-cm incision along the medial thigh was made to reveal the femoral sheath. With blunt and fine-tipped forceps, the femoral sheath was dissected until the femoral artery was exposed. Afterward, vessel loops of 5–0 silk suture were placed along the proximal and distal segments of the femoral artery to control blood flow in the exposed segment. With the use of a Leica M80 stereomicroscope (Leica Microsystems, Heerbrugg, Switzerland), an arteriotomy was created in the center of the exposed segment by using a 26-gauge Angiocath (outer diameter, 0.46 mm; BD Biosciences, San Jose, California). An 8–0 suture (Fine Science Tools, North Vancouver, British Columbia, Canada) was placed on one of the lips created by the arterial puncture for the purpose of facilitating the introduction of a catheter. A custom-preshaped J catheter (Excelsior SL-10 microcatheter; Stryker, Kalamazoo, Michigan) modified to 30 cm in length was introduced into the femoral artery. The catheter was advanced into the

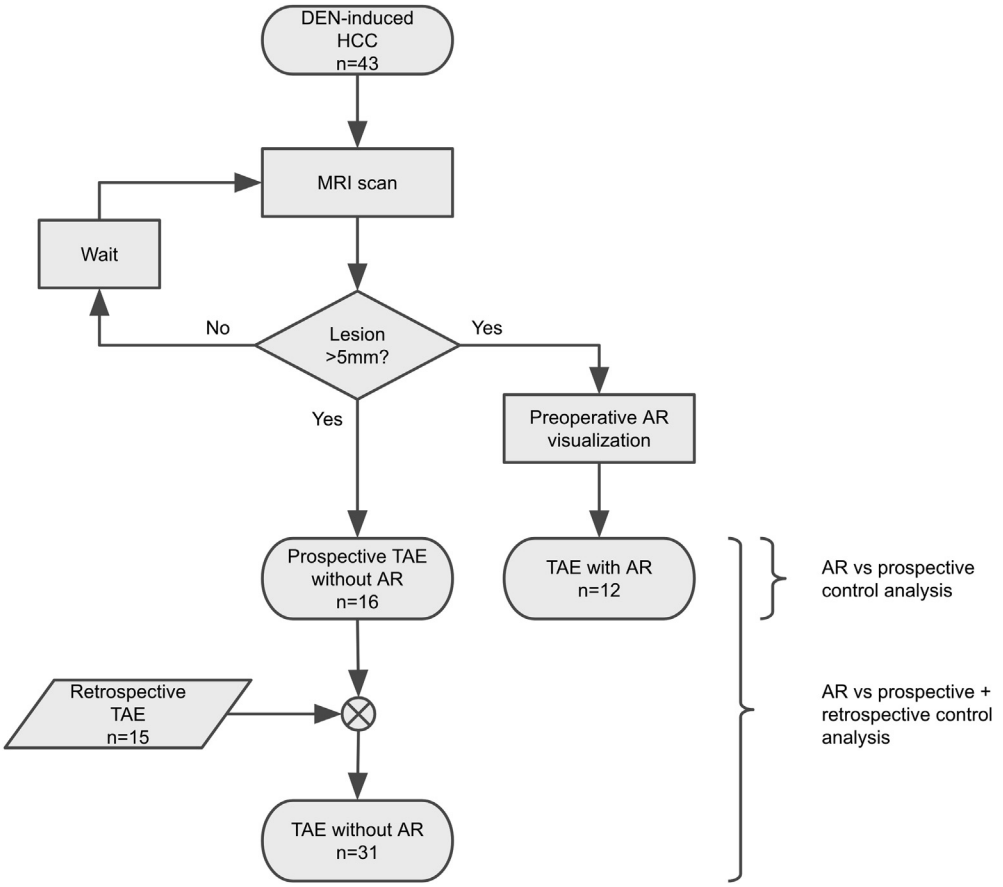

Figure 1. Flowchart of study design. Prospective analysis was performed with and without AR. Retrospective controls were added to improve statistical power and analyzed separately.

femoral artery with the aid of a coaxially inserted 0.010-inch guide wire (Transend guide wire; Stryker). Then, selective catheterization of the celiac artery and arteriography with Omnipaque 300 (0.3 mL; GE Healthcare, Chicago, Illinois) were performed. Superselective catheterization of the segmental hepatic artery supplying the tumor was performed by using a coaxially inserted SAI MTV-40 microcatheter (SAI Infusion Technologies, Lake Villa, Illinois).

Embolization was performed with 0.05 mL of sedimented 40–120-μm Embosphere particles (Merit Medical, South Jordan, Utah) or 40–90-μm LC Bead LUMI particles (BTG, London, United Kingdom) diluted in 0.9 mL of Omnipaque 300 (GE Healthcare). Delivery of the embolic agent was achieved by using a 1-mL polycarbonate syringe via hand injection or a PHD Ultra Syringe Pump (0.15-mL/min rate; Harvard Apparatus, Holliston, Massachusetts) until the endpoint of embolization, stasis in the selected segmental hepatic artery, was achieved. Postembolization arteriography was performed to confirm stasis. Finally, the catheters were removed, and the 8–0 suture placed on the proximal lip of the arteriotomy was used to close the vessel wall. The fascia and skin were then closed with interrupted 5–0 sutures.

In all cases, preprocedural 2D images were reviewed before embolization. In the AR group, preprocedural AR visualization was additionally performed immediately before the start of the procedure. Total femoral artery catheterization time, which includes nonselective and selective catheterization of segmental hepatic arteries; total fluoroscopy time; DAP; and AK were recorded. Total femoral artery catheterization time was used as a proxy for interventional radiology–related procedure time. Microsurgery and cutdown to the femoral artery for access and catheter insertion were not included in the procedure time, as this was highly variable and is not applicable to human cases. Additionally, emphasis was placed on procedural-related tasks directly relevant to preprocedural imaging, and the femoral arteries were not included in the preprocedural MR imaging of the abdomen. Total femoral artery catheterization time was calculated as the interval from the first fluoroscopic image time to the last fluoroscopic image time. This was validated in 6 prospective cases comparing manually recorded catheterization times versus differences in fluoroscopic image time stamps. There was strong correlation between manually recorded times and fluoroscopic image time stamps, with a Pearson correlation coefficient r of 0.99 (**Fig E2** [available online on the article's Supplemental Material page at *www.jvir.org*]).

MR Imaging

Axial and coronal T2-weighted images were acquired with a Varian 4.7-T 40-cm horizontal-bore MR spectrometer with a 25-G/cm gradient tube interfaced to a Varian Direct Drive console (Agilent Technologies, Santa Clara, California). Images of the abdomen were acquired from the lung bases

to the pelvic inlet and did not include the femoral arteries. Sequence parameters included a 70-mm × 70-mm field of view, 2-mm slice thickness, 20 slices, 4 averages, 256 × 256 matrix size, repetition time of 1.5–2 s, and echo time of 60 ms. Of note, intravenous gadolinium contrast medium (total 1 mL with 0.3 mL contrast medium and 0.7 mL saline solution) was administered via tail vein, and postcontrast images were acquired. Rats were anesthetized with isoflurane for the duration of the MR study. Digital Imaging and Communications in Medicine (DICOM) images were exported from the scanner, and 2D slices were sequentially reviewed with ITK-SNAP software (12).

Three-Dimensional Holographic Rendering

Holographic 3D volumes were generated by using 3D texture mapping of the DICOM dataset. T2-weighted MR images were exported from the scanner in DICOM format. Direct volume rendering was performed by using ray casting and optimization techniques with SurgicalAR software (Medivis, Brooklyn, New York) on an Alienware 15 R3 laptop computer with Intel Core i7-7820HK, 32 GB RAM, and GTX 1080 GPU (Dell, Austin, Texas). Rendering was performed locally on the laptop and remotely streamed to a HoloLens AR headset device (Microsoft, Redmond, Washington) in real time via 5-Ghz wireless network. Holographic 3D volume manipulations including rotation, magnification, windowing, and modification of voxel opacities were used during HoloLens visualization. Additionally, an invisible cut plane at a set distance from the headset allowed the volume to be viewed from any perspective angle (**Video 2** [available online on the article's Supplemental Material page at *www.jvir.org*]). AR system setup and operator viewing times were recorded.

Statistical Analysis

Statistical analysis was performed with Google Sheets software (Google, Mountain View, California). Means and variances were compared by Welch t test and F test, respectively. Categoric rat population characteristics were compared by χ^2 test. Outlier analysis was initially performed for values beyond 2 times the interquartile range and omitted from inclusion for comparison. This included the omission of high radiation exposures from one case with AR, including fluoroscopy time, AK, and DAP, in which further investigation revealed that the settings during the case were unintentionally altered between fluoroscopy and digital radiography. Additionally, a high DAP value from one case without AR was omitted. The reason for this high DAP value was unknown, as fluoroscopy time and AK values from this case remained within outlier limits.

RESULTS

Prospective procedural metrics from transarterial embolization procedures are summarized in **Table 2**. AR system setup and operator viewing times measured approximately 3 minutes each, for an average total of 5.9 minutes of additional preprocedure time per case (**Fig 2**). Prospective analysis showed a reduction in total catheterization time, including nonselective and selective catheterization, from 42.7 minutes to 31.0 minutes (27%), after AR that did not reach statistical significance ($P = .11$). A reduction in total fluoroscopy time was also observed, from 11.7 minutes to 7.4 minutes (37%), after AR that did not reach statistical significance ($P = .12$). Likewise, comparisons between the AR and retrospective control groups also revealed reductions in catheterization and fluoroscopy times that did not reach statistical significance (**Table 3**). As expected with decreased fluoroscopy times, there were associated reductions in DAP and AK prospectively (**Table 2**), which did not reach statistical significance. The reduction in DAP was incremental (4%; $P = .83$) compared with the reduction in AK (37%; $P = .13$).

Comparisons between the prospective and retrospective control groups, as shown in **Table 4**, showed no difference in mean catheterization or fluoroscopy times despite the 2-year time difference between the groups ($P = .97$ and $P = .48$, respectively). Additionally, there was no statistically significant difference in the variance in fluoroscopy time between the control groups ($P = .08$). Because the mean and variance in fluoroscopy time between the prospective and retrospective control groups were similar, these control groups were combined to improve statistical power (**Table 5**). The increase in power afforded by combining these control groups allowed the present analysis to demonstrate a significant reduction in fluoroscopy time after AR from 14.1 minutes to 7.4 minutes (48%; $P = .01$; **Fig 3**). In addition, there was a statistically significant difference in the variance in fluoroscopic time prospectively ($P = .02$; **Table 2**), with a reduction in this variation after the use of AR (**Fig 3**). The different angiography systems used for the retrospective and prospective control groups confounded comparisons of radiation exposure.

Table 2. Comparison of Procedural Metrics from Embolization in Rats between AR and Control Prospective Group

Metric	AR (n = 12)	Control Prospective (n = 16)	*P* Value	
			t test	*F* test
Average time (min:s)				
HoloLens setup	3:22	–	–	–
HoloLens use	2:52	–	–	–
Average total time (min)				
Catheterization	31.0	42.7	.11	.21
Fluoroscopy	7.4	11.7	.12	.02*
Average DAP (μGy·m^2)	191	199	.83	.31
Air kerma (mGy)	17.6	28.0	.13	.01*

AR = augmented reality; DAP = dose–area product.
*$P < .05$.

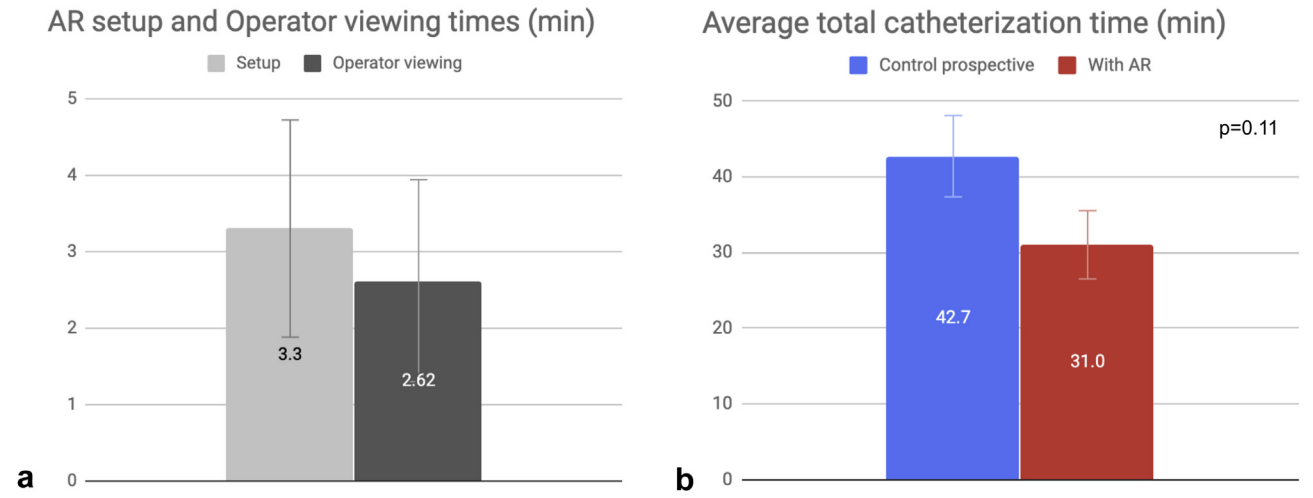

Figure 2. Bar graphs of AR system setup and operator viewing times as well as total catheterization times for prospective embolizations performed with and without AR. **(a)** Setup and operator viewing times were similar. Error bars represent standard deviation. **(b)** A 27% decrease in average total catheterization time was seen ($P = .11$). Error bars represent standard error of the mean.

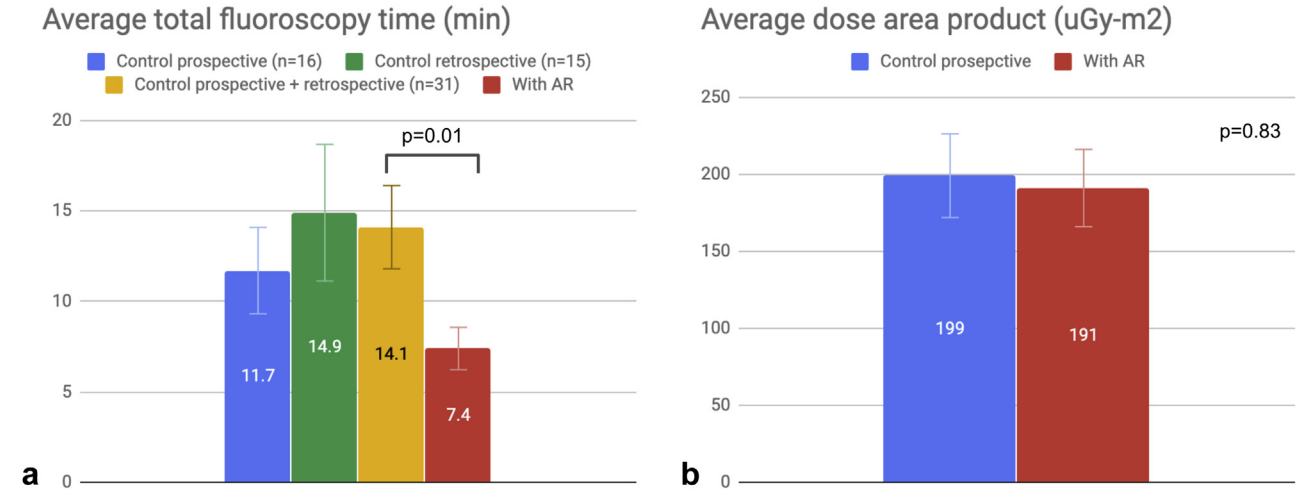

Figure 3. Bar graphs of radiation exposure for embolizations performed with or without AR. Error bars represent standard error of the mean. **(a)** A 36% decrease in total fluoroscopy time was seen with AR compared with prospective controls ($P = .12$). There was no significant difference in fluoroscopy times between prospective and retrospective controls ($P = .48$). A 48% decrease in fluoroscopy time was seen compared with combined prospective and retrospective controls ($P = .01$). Variation narrowed following AR, as shown by the error bars. **(b)** No significant change in DAP was observed ($P = .83$) despite decreased fluoroscopy time.

DISCUSSION

Preprocedural stereoscopic 3D visualization with AR showed a reduction in fluoroscopy time that did not reach statistical significance compared with a prospectively acquired control group, likely because of limited statistical power. As such, a statistically significant reduction in fluoroscopy time was observed after the use of AR compared with combined prospective and retrospective controls. DAP and AK are closely related to fluoroscopy time, and the expected trends in reductions in these values were also present prospectively but did not reach statistical significance. Despite DAP and AK being complementary, the reduction in DAP was incremental, if any, compared with the reduction in AK. This discrepancy in reduction may be partly related to the fact that rats are small and embolizations were performed on angiography systems intended for human use and calibrated with human phantoms.

The reduction in total catheterization time, which includes nonselective and selective catheterization, after AR also did not reach statistical significance. In addition to differences in anatomy on a case-by-case basis, other factors influencing total catheterization time included delivery and type of embolic agent. Embolization was performed with 40–120-μm Embosphere or 40–90-μm LUMI beads, and one may have achieved the endpoint of embolization and vessel stasis more quickly than the other. These factors, among others, may have influenced catheterization time.

Although preprocedural planning time increased slightly with AR, there is a potential for greater savings in

Table 3. Comparison of Procedural Metrics from Embolization in Rats between AR and Control Retrospective Group

Metric	AR (n = 12)	Control Retrospective (n = 15)	*P* Value	
			t test	*F* test
Average total time (min)				
Catheterization	31.0	42.3	.41	.001*
Fluoroscopy	7.4	14.9	.08	.002*
Avg DAP (μGy·m^2)	191	302	.051	.03*
Air kerma (mGy)	17.6	81.6	.001*	.0001*

AR = augmented reality; DAP = dose–area product.
*$P < .05$.

Table 4. Comparison of Procedural Metrics from Embolization in Rats between Control Prospective and Retrospective Groups

Metric	Control Prospective (n = 16)	Control Retrospective (n = 15)	*P* Value	
			t test	*F* test
Average total time (min)				
Catheterization	42.7	42.3	.97	.004*
Fluoroscopy	11.7	14.9	.48	.08
Average DAP (μGy·m^2)	199	302	.07	.04*
Air kerma (mGy)	28.0	81.6	.003*	.003*

DAP = dose–area product.
*$P < .05$.

Table 5. Comparison of Procedural Metrics from Embolization in Rats between AR and Combined Control Prospective and Retrospective Groups

Metric	AR (n = 12)	Combined Control (n = 31)	*P* Value	
			t test	*F* test
Average total time (min)				
Catheterization	31.0	43.1	.12	.01*
Fluoroscopy	7.4	14.1	.01*	.004*
Average DAP (μGy·m^2)	191	251	.13	.05*
Air kerma (mGy)	17.6	56.9	.0002*	.0002*

AR = augmented reality; DAP = dose–area product.
*$P < .05$.

catheterization time, a marker of procedure time, as well as fluoroscopy time to outweigh the increased planning time. Consistent with this benefit, AR was associated with a reduction in variations in fluoroscopy time, suggesting that AR may be helpful in preventing excessive fluoroscopy use. For endovascular procedures, 3D visualization may aid in the understanding of where to precisely position the catheter and result in decreased fluoroscopy times; however, actually advancing the catheter to that position may be influenced by a variety of factors that can diminish the associated improvements in procedural metrics, including but not limited to operator experience, available catheters and wires, and angles of branching vessels. Nevertheless, these findings demonstrate the potential quantitative and tangible benefits of AR that are necessary to motivate clinical trials.

The potential benefits of 3D AR visualization of preprocedural imaging before embolization may be multifactorial. Three-dimensional AR visualization has been shown to decrease mental task load during simulated surgery (13). Despite the unknown cognitive mechanism, benefits from holographic 3D visualization could have real value. In addition, the freedom and ease to visualize the volume with AR in any plane and from any perspective angle may provide insight into optimal positioning of the C-arm detector during the procedure, thereby decreasing vessel selection time and fluoroscopy time. As shown in **Video 2** (available online on the article's Supplemental Material page at *www.jvir.org*), particularly when the holographic 3D volume is visualized in the coronal orientation, the AR headset can simulate C-arm positioning and help establish relationships of the target relative to the spine or other lesions in the liver. The operator can also obtain a better 3D depiction of the catheter course needed for vessel selection, which may be difficult to ascertain from scrolling through preprocedural images on a 2D monitor screen. As a result, not only can the operator obtain an improved practical sense of anatomy preprocedurally, but this greater sense of anatomic understanding in relation to other structures can manifest as an ancillary aid and facilitate innate recall during tasks in the procedure. Along these lines, and based on studies of 3D printed models for surgical planning (3–5), smoother and faster procedures with decreased fluoroscopy use would be anticipated with improved planning, recall, and anatomic understanding. Ultimately, improved anatomic understanding after AR may give the operator enough confidence to forego cone-beam CT during the procedure, thereby saving procedure time and radiation exposure. Although AR was used only in the preprocedural planning phase in the present study, intraprocedural 3D AR may also potentially benefit procedural metrics (**Fig E1** and **Video 1** [available online on the article's Supplemental Material page at *www.jvir.org*]).

Limitations of the present study include its single-center nature and the use of prospective and retrospective data for analysis. Prospective comparisons showed changes in procedural metrics that did not reach statistical significance. As the study was determined to be underpowered, retrospective controls were analyzed and combined to increase statistical power. Additionally, even though the operators may have become more efficient and able to selectively catheterize arteries faster over time with experience, there was no difference in mean catheterization time or fluoroscopy time between the prospective and retrospective control groups. This absence of improvement argues against benefits from increased operator experience with time. Moreover, both operators have been performing embolizations in rats in a similar fashion since 2014. In

addition, implicit bias may exist from merely the use of AR, which is difficult to control. The possibility remains that, by simply donning the headset, the operator may have been compelled to perform the procedure more quickly or use less fluoroscopy. Also, the complexity of cases (eg, variant anatomy, multiple feeding vessels) was not analyzed or taken into account, which would impact catheterization time and fluoroscopy use.

In conclusion, the present study suggests that AR may provide immediate benefit in endovascular procedures by enabling reduced and more consistent catherization and fluoroscopy times. Further studies should be performed to evaluate the potential of AR on endovascular oncologic interventions.

ACKNOWLEDGMENTS

B.P. received grants from the National Institutes of Health (5T32EB004311), Society of Interventional Radiology Foundation, and Radiological Society of North America Research and Education Foundation. The authors thank the Penn Medicine Medical Device Accelerator for supporting equipment for this research.

REFERENCES

1. Sutherland J, Belec J, Sheikh A, et al. Applying modern virtual and augmented reality technologies to medical images and models. J Digit Imaging 2018; 32:38–53.
2. Uppot RN, Laguna B, McCarthy CJ, et al. Implementing virtual and augmented reality tools for radiology education and training, communication, and clinical care. Radiology 2019; 291:570–580.
3. Mitsouras D, Liacouras P, Imanzadeh A, et al. Medical 3D printing for the radiologist. Radiographics 2015; 35:1965–1988.
4. Tack P, Victor J, Gemmel P, Annemans L. 3D-printing techniques in a medical setting: a systematic literature review. Biomed Eng Online 2016; 15:115.
5. Perica ER, Sun Z. A systematic review of three-dimensional printing in liver disease. J Digit Imaging 2018; 31:692–701.
6. Yammine K, Violato C. A meta-analysis of the educational effectiveness of three-dimensional visualization technologies in teaching anatomy. Anat Sci Educ 2015; 8:525–538.
7. Mohammed MAA, Khalaf MH, Kesselman A, Wang DS, Kothary N. A role for virtual reality in planning endovascular procedures. J Vasc Interv Radiol 2018; 29:971–974.
8. Miyayama S, Yamashiro M, Sugimori N, Ikeda R, Okimura K, Sakuragawa N. Outcomes of patients with hepatocellular carcinoma treated with conventional transarterial chemoembolization using guidance software. J Vasc Interv Radiol 2019; 30:10–18.
9. Karmonik C, Elias SN, Zhang JY, et al. Augmented reality with virtual cerebral aneurysms: a feasibility study. World Neurosurg 2018; 119: e617–e622.
10. Gade TP, Hunt SJ, Harrison N, et al. Segmental transarterial embolization in a translational rat model of hepatocellular carcinoma. J Vasc Interv Radiol 2015; 26:1229–1237.
11. Kiefer RM, Hunt SJ, Pulido S, et al. Relative initial weight is associated with improved survival without altering tumor latency in a translational rat model of diethylnitrosamine-induced hepatocellular carcinoma and transarterial embolization. J Vasc Interv Radiol 2017; 28: 1043–1050.e2.
12. Yushkevich PA, Piven J, Hazlett HC, et al. User-guided 3D active contour segmentation of anatomical structures: significantly improved efficiency and reliability. NeuroImage 2006; 31: 1116–1128.
13. Fotouhi J, Fuerst B, Lee SC, et al. Interventional 3D augmented reality for orthopedic and trauma surgery. Presented at the 16th Annual Meeting of the International Society for Computer Assisted Orthopedic Surgery, June 8–11, 2016; Osaka, Japan.

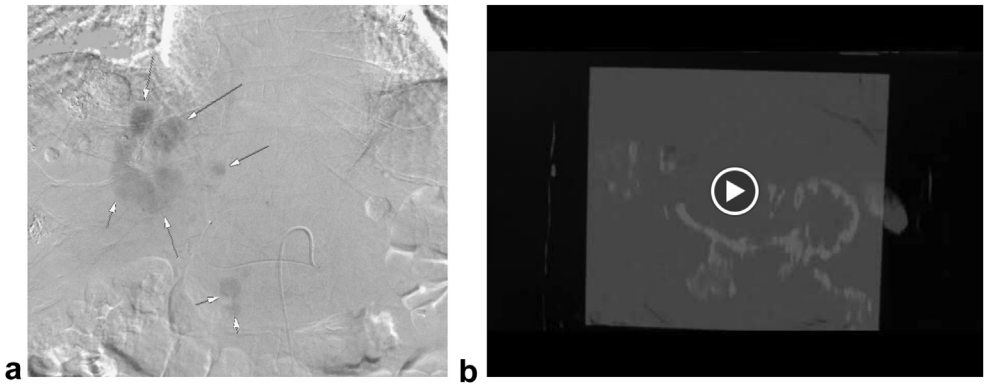

Figure E1. Integration of preprocedural 3-dimensional (3D) magnetic resonance (MR) imaging with live fluoroscopy with an augmented reality (AR) headset device. **(a)** Digital subtraction hepatic arteriogram shows multiple hypervascular tumors (arrows) corresponding to multifocal hepatocellular carcinoma (HCC). **(b)** Holographic 3D rendering of preprocedural MR imaging visualized over the live monitor screen. Anteroposterior locations of the tumors are much more evident.

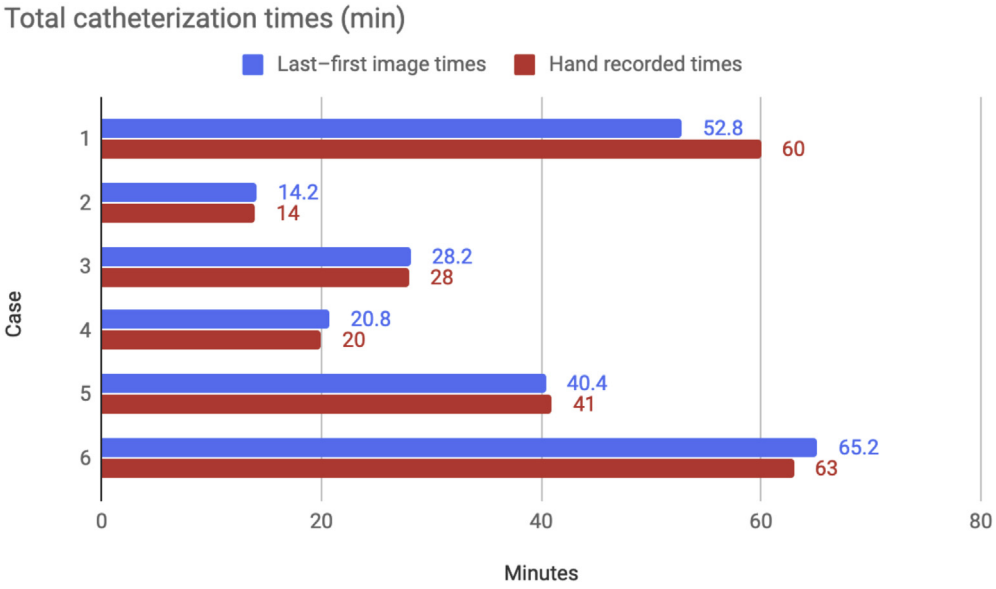

Figure E2. Validation of measurement of total femoral artery catheterization times in 6 prospective cases. A strong correlation (Pearson correlation coefficient $r = 0.99$) was seen between hand-measured catheterization times recording the times of insertion and withdrawal of the catheter from the femoral artery and catheterization times calculated between the first and last fluoroscopic image time stamps.